



# Colliding respiratory jets as a mechanism of air exchange and pathogen transport during conversations

Arghyanir Giri<sup>1</sup>, Neelakash Biswas<sup>1,2</sup>, Danielle L. Chase<sup>3</sup>, Nan Xue<sup>3</sup>,  
Manouk Abkarian<sup>4</sup>, Simon Mendez<sup>5,†</sup>, Sandeep Saha<sup>1,†</sup> and  
Howard A. Stone<sup>3,†</sup>

<sup>1</sup>Department of Aerospace Engineering, Indian Institute of Technology Kharagpur, West Bengal 721302, India

<sup>2</sup>Department of Aeronautics, Imperial College London, Exhibition Road, London SW7 2AZ, UK

<sup>3</sup>Department of Mechanical & Aerospace Engineering, Princeton University, Princeton, NJ 08544, USA

<sup>4</sup>Centre de Biochimie Structurale, CNRS UMR 5048–INSERM UMR 1054, University of Montpellier, 34090 Montpellier, France

<sup>5</sup>Institut Montpellierain Alexander Grothendieck, CNRS, University of Montpellier, 34095 Montpellier, France

(Received 8 August 2021; revised 28 September 2021; accepted 10 October 2021)

Air exchange between people has emerged in the COVID-19 pandemic as the important vector for transmission of the SARS-CoV-2 virus. We study the airflow and exchange between two unmasked individuals conversing face-to-face at short range, which can potentially transfer a high dose of a pathogen, because the dilution is small when compared to long-range airborne transmission. We conduct flow visualization experiments and direct numerical simulations of colliding respiratory jets mimicking the initial phase of a conversation. The evolution and dynamics of the jets are affected by the vertical offset between the mouths of the speakers. At low offsets the head-on collision of jets results in a ‘blocking effect’, temporarily shielding the susceptible speaker from the pathogen carrying jet, although, the lateral spread of the jets is enhanced. Sufficiently large offsets prevent the interaction of the jets. At intermediate offsets (8–10 cm for 1 m separation), jet entrainment and the inhaled breath assist the transport of the pathogen-loaded saliva droplets towards the susceptible speaker’s mouth. Air exchange is expected, in spite of the blocking effect arising from the interaction of the respiratory jets from the two speakers.

**Key words:** jets, particle/fluid flow, turbulent mixing

† Email addresses for correspondence: [simon.mendez@umontpellier.fr](mailto:simon.mendez@umontpellier.fr), [ssaha@aero.iitkgp.ac.in](mailto:ssaha@aero.iitkgp.ac.in), [hastone@princeton.edu](mailto:hastone@princeton.edu)

© The Author(s), 2021. Published by Cambridge University Press. This is an Open Access article, distributed under the terms of the Creative Commons Attribution licence (<http://creativecommons.org/licenses/by/4.0/>), which permits unrestricted re-use, distribution, and reproduction in any medium, provided the original work is properly cited.

## 1. Introduction

As the world emerges from the COVID-19 pandemic, many people are resuming ordinary activities. Because it is now well recognized that the SARS-CoV-2 virus is transmitted by an airborne route, and predominantly via aerosol droplets, there have been significant efforts in enhancing ventilation as a public health strategy (Bhagat & Linden 2020; Bhagat *et al.* 2020; Morawska & Cao 2020; Bazant & Bush 2021; Poydenot *et al.* 2021). This is particularly effective for decreasing the amount of virus suspended in aerosols that may accumulate in indoor air over minutes or hours. However, in unmasked conversations, air exchanges over a distance of 1 m probably begin to occur in a few seconds (Abkarian *et al.* 2020) and potentially transmit a significant dose of pathogen via aerosol (Fennelly 2020; Prather, Wang & Schooley 2020; Prather *et al.* 2020; Greenhalgh *et al.* 2021) due to limited dilution. It is thus important to understand the possible transmission in conversations, which are likely to be the most frequent form of social interactions; more contagious variants emphasize the possible role of this transmission route. Thus, we use numerical simulations, and corresponding qualitative laboratory experiments, to highlight such airflows and clarify the mechanism of air exchanges at relatively short distances.

Airborne transmission can occur via short- and long-range routes (Morawska *et al.* 2020; Tang *et al.* 2021). The latter largely concerns ventilation and has been the subject of numerous investigations (Bhagat & Linden 2020; Bhagat *et al.* 2020; Klompas, Baker & Rhee 2020; Morawska & Cao 2020; Allen & Ibrahim 2021; Bazant & Bush 2021; Mathai *et al.* 2021; Ng *et al.* 2021; Poydenot *et al.* 2021). For example, long-range transmission is responsible for most super-spreading events. In contrast, short-range transmission consists of coughs, sneezes or direct inhalation of exhaled air from an infected person. The potential of a short-range airborne route to transmit large doses in a short period is acknowledged (Poydenot *et al.* 2021; Tang *et al.* 2021), although generally it has not been quantified. Transmission via coughs and sneezes has been investigated (Bourouiba 2020, 2021; Chong *et al.* 2021), but face-to-face conversations (see [figure 1a](#)) have received less attention (Abkarian *et al.* 2020; Yang *et al.* 2020; Singhal *et al.* 2021). Unlike sneezing or coughing ( $1\text{--}10^3$  particles per second), speaking and breathing generally produce small droplets but in significant quantity ( $1\text{--}10^4$  particles per second) (Asadi *et al.* 2020; Pöhlker *et al.* 2021). In addition, in COVID-19 the viral load from the upper airways of infected people is high the day before the onset of symptoms, so asymptomatic spreading accounts for a significant share of transmissions (Anderson *et al.* 2020; Prather *et al.* 2020). These facts emphasize the need for analysing the local flow environment and air exchange during a conversation.

We focus on short-range airborne transmission via unmasked face-to-face conversations that occur in meetings, social gatherings, restaurants, etc. Such a configuration is complex, and our present understanding is impeded by the spectrum of physical phenomena involved, ranging from microbiology, human phonetics and aerosolization of droplets (Pöhlker *et al.* 2021), apart from the fluid mechanics that involves exhaled jets, turbulent interaction of colliding jets and interaction with background flows. The complex airflows created by exhalation and inhalation during human speech have characteristics of both continuous and pulsating jets and are dominated by a train of vortical puffs and conical jet-like flows (Gupta, Lin & Chen 2010; Abkarian *et al.* 2020; Yang *et al.* 2020). In a typical conversation between two people in a social setting ([figure 1a](#)), the jet-like flow produced by one individual is modulated by the flow exhaled by the second individual. In such an interaction, the rapid evolution of flow structures and the corresponding droplet dispersal process remain unexplored. In addition to identifying the fundamental transport mechanisms of pathogens in conversations, quantifying the air exchanges may inform

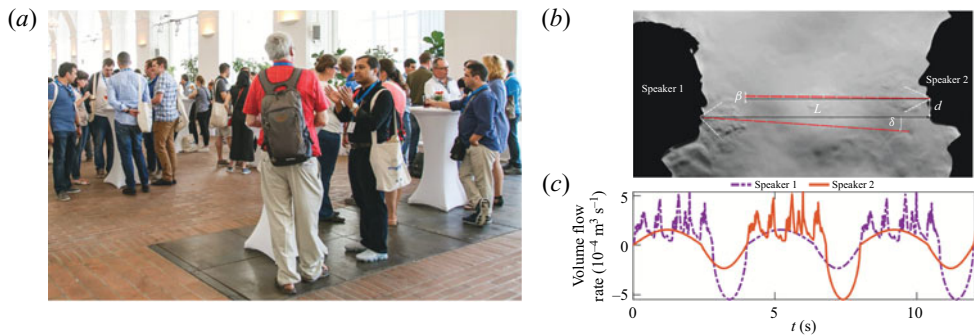


Figure 1. (a) A social gathering with people speaking to each other in close proximity. (b) Two people facing each other during a conversation (snapshot from the supplementary movie S4 of Tang *et al.* 2011) at a distance  $L$  with mouth offset height  $d$ . The offset angle  $\theta = \beta - \delta$ , where  $\delta$  and  $\beta$  are the angles between the jet centrelines and the horizontal direction from speakers 1 and 2, respectively. The jet centreline is approximated as the bisector of the angle subtended at the lips. (c) Typical volume flow-rate signals used in simulations for phrase ‘S’ (see below). The signal for speaker 2 lags that of speaker 1 by 4 s.

coarse-grained models that estimate transmissions in crowds (Garcia *et al.* 2021), which feature spatial models of transmission risks. Such models rely on a prediction of droplet inhalation depending on the orientation and distance with respect to an infectious source, but the effect of the breathing and speaking of a susceptible person is currently neglected due to the lack of data and the knowledge of how airflows interact.

We study the interaction between two colliding jet-like flows, produced due to breathing and speaking, through direct numerical simulations (DNS) and flow visualization experiments. Interactions of turbulent jets have been studied in applications such as combustion (Rolon *et al.* 1991), heat and mass transfer (Besbes *et al.* 2003; Li *et al.* 2008; Liu *et al.* 2009) and geophysical flows (Denshchikov, Kondrat’ev & Romashov 1978; Kaye & Linden 2006). In most of the studies the primary interest has been the zone where the jets collide, whereas our main focus is on the flow that reaches the jet origin at the other end after the collision. Also, in previous studies the length scales considered are different from those encountered in a typical conversation. For instance, in most studies (Denshchikov *et al.* 1978; Rolon *et al.* 1991; Besbes *et al.* 2003; Li *et al.* 2008; Liu *et al.* 2009), the ratio between the separation distance and the nozzle diameter is small ( $<25$ ) unlike in a conversation, for which the ratio between the separation distance ( $L$ ) and mouth diameter can be  $\sim 40$  at a separation of 1 m. Further, a typical conversation introduces additional parameters, such as the offset height ( $d$ ), breathing/speaking time scale and the phase difference of the conversation ( $\psi$ ), which are not considered in other problems of interacting turbulent jets. The natural variability of the parameters introduces additional complexity, and drawing physical, as opposed to quantitative, conclusions seems appropriate at this stage.

Further, we make a number of simplifications in order to gain insight into the mechanisms at play during a face-to-face conversation. For instance, we consider the effects of parameters like the separation distance between the speakers  $L$ , the offset height  $d$  (speakers can be of different heights, whether standing or sitting) and the type of conversation through different spoken phrases and the phase difference ( $\psi$ ) in a conversation. Figure 1(b) shows a snapshot of the supplementary movie S4 of Tang *et al.* (2011), where two people converse at a separation distance  $L$  ( $\sim 1$  m) and height offset  $d$ . It is also plausible to encounter an angle offset (the angle between the centrelines of

the two exhaled jets) that might influence the interaction. In [figure 1\(b\)](#) the offset angle,  $\theta$ , is defined as  $\beta - \delta$ , where  $\delta$  and  $\beta$  are the angles between the jet centrelines and the horizontal directions of speakers 1 and 2, respectively. The jet centreline is approximated as the bisector of the angle subtended at the lips. However, at a separation distance  $L \geq 1$  m, the offset angle can be small ([Tang et al. 2011](#)) (for details, see § 4 in the supplementary material, available at <https://doi.org/10.1017/jfm.2021.915>). We assume the breathing and speech time scales to be approximately 4 s, following [Abkarian et al. \(2020\)](#), and the volume flow rate is assumed to be 0.5 litre per breathing cycle.

Two findings of our study appear particularly significant when interpreted with social distancing guidelines relevant to mitigating pathogen spread: (i) At small offsets, blocking occurs due to collision of the jets, and increasing the offset diminishes the blocking. The blocking reduces the risk of direct transmission to speaker 2 at low offsets, although the enhanced lateral spread of the jets at low offsets may increase the risk of transmission to individuals standing nearby. (ii) For typical conditions of conversations, there exists a critical window of offsets where the droplets carried by a jet invade the vicinity of the second speaker approximately a metre away within tens of seconds, and the risk of transmission increases monotonically thereafter. Phonetic features of speech, such as plosives, likely extend the interaction distance and reduce the necessary contact time.

## 2. Air exchange

### 2.1. The blocking effect

Typical volumetric flow-rate signals used in our three-dimensional numerical simulations for two individuals – speaker 1 (e.g. infected) and speaker 2 (e.g. susceptible) – speaking one at a time are shown in [figure 1\(c\)](#). For speaker 1, the first 4 s of the signal correspond to the phrase ‘Sing a song of sixpence’ (phrase ‘S’) and the next 4 s to a breath-like signal ([Abkarian et al. 2020](#)). Simulations were also performed with the phrase ‘Peter Piper picked a peck’ (phrase ‘P’). To simulate a conversation, a phase difference,  $\psi$ , defined as the time difference between the instants at which speakers 1 and 2 initiate speech, of 4 s has been introduced: when 1 speaks, 2 breathes and *vice versa*.

Simulations are performed for offset heights  $d = 0$ –10 cm and separation distances  $L = 1$ –1.5 m (see § 1 in the supplementary material for details). Simulations are also performed with other values of  $\psi$  for  $d = 0$  to elucidate the effects of the phase difference. The mouth is modelled as an elliptical orifice with semi-major axis ( $a$ ) and semi-minor axis ( $b$ ) 1.5 cm and 1 cm, respectively. We inject tracers from the mouth (see § 1 in the supplementary material) and their evolution is tracked to assess the behaviour of the smallest emitted droplets. Indeed, during speech, submicrometre- to millimetre-size particles are emitted ([Duguid 1946](#); [Bourouiba 2021](#); [Pöhlker et al. 2021](#)). Large particles (100  $\mu\text{m}$ ) are significantly influenced by gravity ([Chong et al. 2021](#)), and millimetre-size particles even have ballistic trajectories ([Bourouiba 2021](#)). However, most particles emitted by speech are of the order of 1  $\mu\text{m}$  in diameter ([Asadi et al. 2020](#); [Pöhlker et al. 2021](#)), a size for which the assumption that particles follow the fluid as tracers is relevant. To support this statement, we calculate the Stokes number,  $St = \rho_p d_p^2 / (18\mu\tau)$ , where  $\rho_p$  denotes the particle density and  $d_p$  its diameter,  $\mu$  is the air viscosity and  $\tau$  is a typical flow time. In the context of speech, the characteristic time of the flow-rate fluctuations is of the order of  $\tau = 0.1$  s ([Abkarian et al. 2020](#)), so that  $St \approx 3 \times 10^{-5}$  for  $d_p = 1$   $\mu\text{m}$ . Such particles have negligible inertia. In addition, gravity effects are also negligible: during a

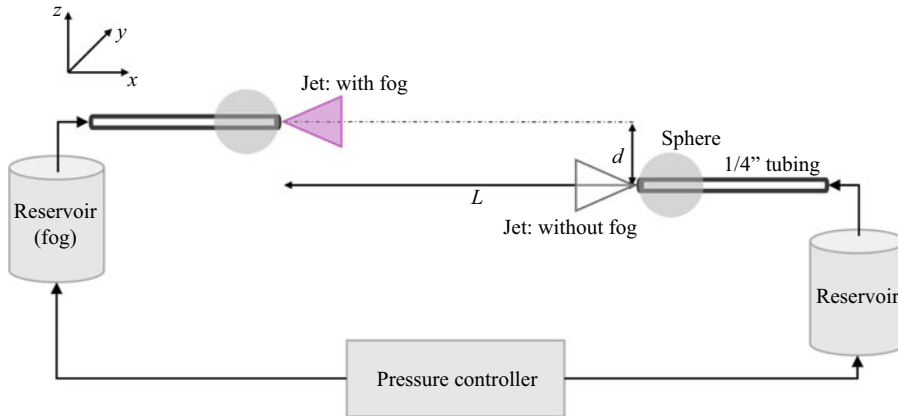


Figure 2. Experimental set-up. Two spheres are placed an axial distance  $L$  apart with a transverse offset  $d$ . A reservoir supplies pressurized air, set by a pressure controller, to the tubing, which goes through the hollow sphere. One reservoir is seeded with fog for visualization of the jet using a laser sheet in the  $xz$ -plane.

30 s conversation as computed here, we estimate a vertical fall of 1 mm for a droplet with  $d_p = 1 \mu\text{m}$ . The analysis based on tracers is thus relevant for most particles emitted by speech.

Buoyancy could affect the trajectory of the particles in some scenarios (Chong *et al.* 2021). However, we are interested in scenarios like the laboratory-scale experiments of Abkarian *et al.* (2020), which have shown that thermal effects are often not significant. The experiments were conducted at room temperature, corresponding to a temperature difference  $\Delta T \sim 10\text{--}15^\circ\text{C}$ . Thermal effects were negligible, most probably due to the enhanced mixing due to turbulent eddies – for instance, see supplementary movie S4 of Abkarian *et al.* (2020), which corresponds to the phrase analysed in our simulations. In our simulations, the peak Reynolds number ( $Re$ ), based on the orifice diameter, is in the range  $Re \approx 1800\text{--}2100$  during speaking for phrases ‘S’ and ‘P’, respectively, and  $Re \approx 1000$  while breathing, while the average  $Re$  (based on cycle-averaged velocity) for both the phrases is  $\approx 700$ .

To complement the simulations, we performed flow visualization experiments using a set-up that is a scaled model of the simulations, as shown in figure 2. The Reynolds number is comparable to the simulations, with value approximately 700. The axial distance between the orifices is  $L = 25$  cm. Experiments for four transverse offset distances were performed:  $d = 0, 0.625, 1.25$  and  $2.5$  cm. A pressure controller is used to supply pressurized air from two reservoirs to tubing with a diameter of 0.64 cm. One of the reservoirs is seeded with fog for visualization of the jet in the  $xz$ -plane using a laser sheet that illuminates the centre plane of the jet ( $y = 0$ ).

We present flow visualization images in figure 3(a–d) at  $t = 0.75$  s at different non-dimensional offset heights  $d_n \equiv 2d/(L \tan \alpha)$ , where  $\alpha = 11.8^\circ$  is the half-angle of a single exhaled jet; see supplementary movies 1–4. The jet half-angle is calculated by simulation using a cone inside which 90 % of the injected tracer particles reside, similar to Abkarian *et al.* (2020). The time instant is chosen such that the location of the leading edge of the jets at different offsets can be distinguished. For an isolated speaker, the jet (figure 3a) proceeds fastest since there is no obstruction, while the axial propagation of the two-speaker jets is slowed by the collision. We deduce from figure 3(b–d) that the offset height  $d_n$  is a critical parameter for determining the streamwise location of the

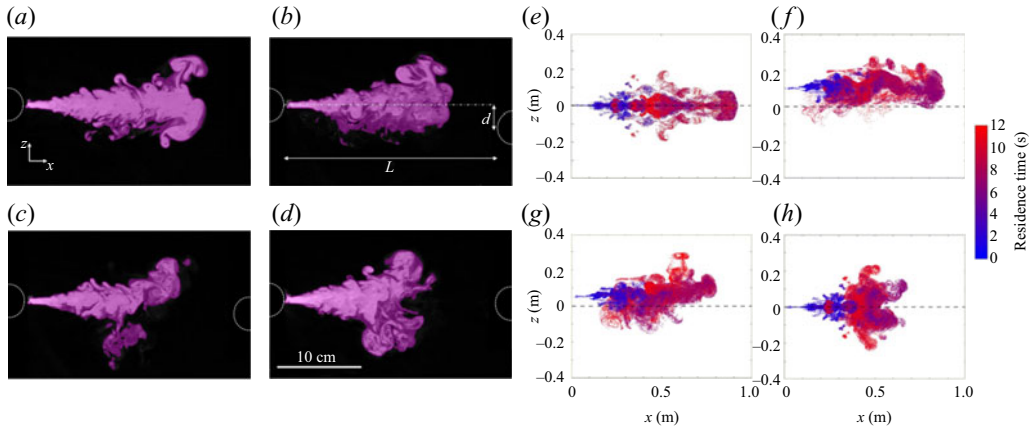


Figure 3. Colliding jets typical of the early time in a conversation. (a–d) Experimental images of a jet for  $Re \approx 700$ ,  $L = 25$  cm at  $t = 0.75$  s, for varying non-dimensional offset height  $d_n$ : (a) free jet (movie 1), (b)  $d_n = 0.95$  (movie 4), (c)  $d_n = 0.48$  (movie 3), and (d)  $d_n = 0$  (movie 2). All supplementary movies are available at <https://doi.org/10.1017/jfm.2021.915>. (e–h) Numerical simulations showing the effect of non-dimensional offset height  $d_n$  on the axial displacement of the particle cloud at  $t \approx 12$  s for  $L = 1$  m: (e) single jet (movie 7), (f)  $d_n = 0.95$  (movie 5), (g)  $d_n = 0.48$  (movie 9), and (h)  $d_n = 0$  (movie 8). The speaking signal used in the simulations corresponds to phrase ‘S’. The particles are colour-coded based on the residence time.

leading edge of an exhaled jet. The collision splits the jets into a two-lobe structure, thus reducing the streamwise spread and enhancing the lateral spread, a phenomenon we term the ‘blocking effect’. The collision is strongest for  $d_n = 0$ , while for the largest vertical separation corresponding to  $d_n = 0.95$ , the exhaled jet closely resembles a single jet, with minimal interaction.

For the corresponding simulations, we inject particles for only one speaker and colour-code the particles by the residence time. Simulations at comparable Reynolds numbers reveal a particle cloud distribution similar to the experiments (figure 3e–h) for the same non-dimensional offset heights, in spite of the differences in the length scales and volume flow-rate signals (Abkarian *et al.* 2020). When speaker 2 does not participate in the conversation (figure 3e), the particle cloud from speaker 1 reaches the proximity of speaker 2 in the shortest time ( $\approx 0.9$  m in approximately 12 s). At larger offset heights, the collision of the jets remains minimal (figure 3f), similar to the experiments. However, at smaller offsets (figure 3g–h), when speaker 2 participates, the exhaled flow shields the region proximal to the face at these relatively short times, due to the blocking effect.

## 2.2. Effect of separation and vertical offset on axial and lateral spread

The changeover of the signal from speaking to breathing also influences the propagation of the leading edge of the jet (see movie 5). Initially the particles released earliest, corresponding to the speaking signal, proceed further but they decelerate and come to a halt due to the loss of momentum to the surrounding fluid. Thereafter, for the conditions of this simulation, the particles released during the breathing signal overtake the earlier exhalations to be the first arrivals in the proximity of speaker 2 (figure 3e–h). Thus, we can see that the spatio-temporal dynamics of a sequence of puff-like signals, i.e. speaking versus breathing, each with its own vortical characteristics that affect longitudinal and lateral spreading, are important to understand the particle transport in the jet profiles.

We present experimental data documenting the axial and lateral spread of the colliding jets for various offsets to quantitatively assess the effect of offset height (figure 4a–c). The

## Air exchange and pathogen transport during conversations

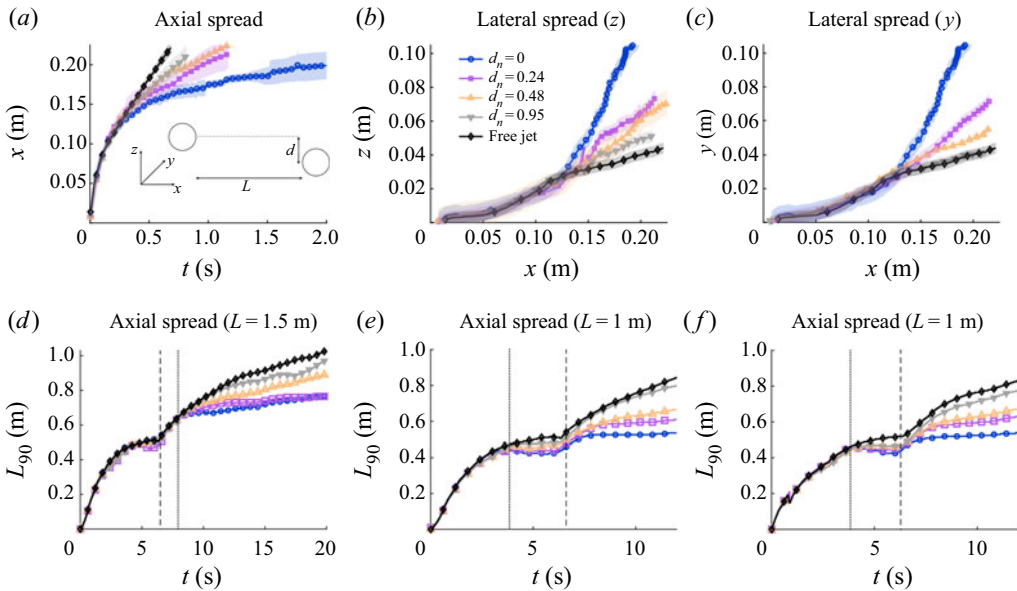


Figure 4. Quantifying the effect of offset height. (a) Experimental jet propagation in the  $x$ -direction as a function of time for varying non-dimensional offset heights  $d_n$ . Inset: schematic, where  $L$  is the separation and  $d$  is the offset between the spheres. (b,c) Extent of the jet in (b) the  $z$ -direction and (c) the  $y$ -direction as a function of downstream distance  $x$ . (d,e) Streamwise length ( $L_{90}$ , from numerical simulations) versus time for phrase ‘S’ at (d) separation of 1.5 m and (e) separation of 1 m. (f) Streamwise length  $L_{90}$  for phrase ‘P’ at a separation of 1 m from numerical simulations. For (d–f) the dashed line and the dotted line represent ‘take-over time’ and ‘collision time’, respectively.

blocking effect is clearly evident in [figure 4\(a\)](#), which shows a sharp reduction in axial penetration of the jet with time as the offset is reduced. The lateral spreading as a function of the downstream location ( $x$ ) is presented in [figure 4\(b,c\)](#). A colliding jet with  $d_n = 0$  has the highest lateral spreading rate due to the collision, while the jet from an isolated speaker has the smallest lateral spread (see also [figure 3](#)).

The axial spreads of the jets obtained from the numerical simulations for different separation distances and spoken phrases ([figure 4d–f](#)) reveal a trend qualitatively similar to the flow visualization experiments. We identify the location of the leading edge in the simulations by defining  $L_{90}$ , which is the axial distance within which 90% of the injected particles reside (Abkarian *et al.* 2020). In [figure 4\(d\)](#), for  $L = 1.5$  m and the spoken phrase ‘S’, we show the evolution of the leading edge. The effect of the changeover of the signal from speaking to breathing is evident from the sharp rise in  $L_{90}$  approximately at  $t = 6.8$  s. This time instant when the exhalation puff overtakes the speech puff is called the ‘take-over time’ and is represented by the dashed lines in [figure 4](#). The  $L_{90}$  values of all of the different offsets almost coincide until approximately at  $t = 7.8$  s, where the two opposing jets are about to collide. This time instant is called the ‘collision time’ and is denoted by the dotted lines in [figure 4](#). After collision, the  $d_n = 0$  case deviates the most from the free-jet evolution due to the blocking effect, similar to the experiments.

In addition, we studied whether changing the separation distance has a significant impact. Keeping the non-dimensional offset values the same as we reduce the separation distance ( $L$ ) to 1 m ([figure 4e](#)), the qualitative trend of  $L_{90}$  remains similar to [figure 4\(d\)](#). The results show that the non-dimensional offset height  $d_n$  is a robust parameter for characterizing the two jet interactions across different combinations of physical separation

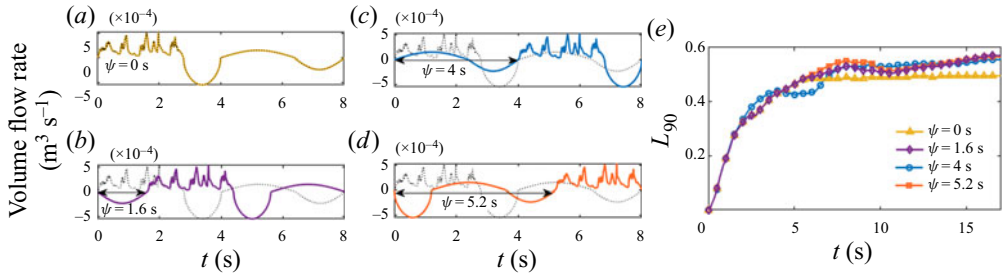


Figure 5. The effect of phase lag on the streamwise propagation of the particle cloud. (a–d) The dotted line represents the volume flow-rate signal of speaker 1 and the solid coloured lines are for speaker 2 with the phase lag  $\psi$  as indicated in the panels. (e) The streamwise length ( $L_{90}$ ) versus time for phrase ‘S’ is shown for phase lags  $\psi = 0$ –5.2 s.

and actual offset heights. Of course, for  $L = 1$  m separation, collision happens earlier at  $\approx 3.9$  s and the collision is stronger compared to that for  $L = 1.5$  m, as evident from a dip in  $L_{90}$  for low offset values ( $d_n = 0$ –0.48) after collision time. Note that, in spite of the complexity of the different simulations, the ‘take-over time’, which is determined by the speaking–breathing signal, remains mostly unaltered.

To understand the effects of the type of conversation, we replace the spoken phrase ‘S’ with phrase ‘P’ in our simulations. In the kinds of simulations reported here, the variation of  $L_{90}$  with time for phrase ‘P’ in figure 4(f) reveals little difference with that obtained for phrase ‘S’ (figure 4e) at the same  $L$  and  $d_n$ . Nevertheless, the role that plosives play in transport can be significant (Abkarian *et al.* 2020), and the details needed to capture these effects are not accounted for in the present simulations.

Note from figure 1(c) that, although the two speakers breath and speak with a phase difference  $\psi = 4$  s, corresponding to the time difference between speakers 1 and 2 initiating speech, their exhalation and inhalation are almost synchronized. We next ask how the streamwise propagation of the exhaled jet changes if the two speakers do not exhale/inhale at the same time (figure 5). Thus, simulations were performed for different values of  $\psi$  for the spoken phrase ‘S’ at  $L = 1$  m and  $d_n = 0$ . These simulations are for the cases for which: speaker 1 exhales (during speaking) and speaker 2 also exhales (during speaking),  $\psi = 0$  s (figure 5a); speaker 1 exhales (during speaking) and speaker 2 inhales (during breathing),  $\psi = 1.6$  s (figure 5b); and speaker 1 exhales (during speaking) while speaker 2 inhales (during speaking),  $\psi = 5.2$  s (figure 5d). We compare the axial spreading with the case reported previously in figure 4(e) for  $d_n = 0$ , i.e.  $\psi = 4$  s (figure 5c). The  $L_{90}$  values for these cases are reported in figure 5(e). For the hypothetical case (figure 5a), i.e. when both the speakers speak and breath exactly in phase, the jet effectively stagnates at  $x = 0.5$  m, while for the other three cases, for which the phase lag is non-zero, the jet penetrates further. However, the difference in the axial spreading rate of cases with non-zero phase lag is not significant; the take-over time and the collision time are affected only slightly. The blocking effect still persists because the time scale for a jet to reach the other speaker at  $L = 1$  m is an order of magnitude higher than the time scale of inhalation/exhalation.

### 2.3. Critical offset window

Finally, we utilize this understanding of the flow to qualitatively assess the relative risk of virus transmission for different offset scenarios. It is expected that the blocking effect

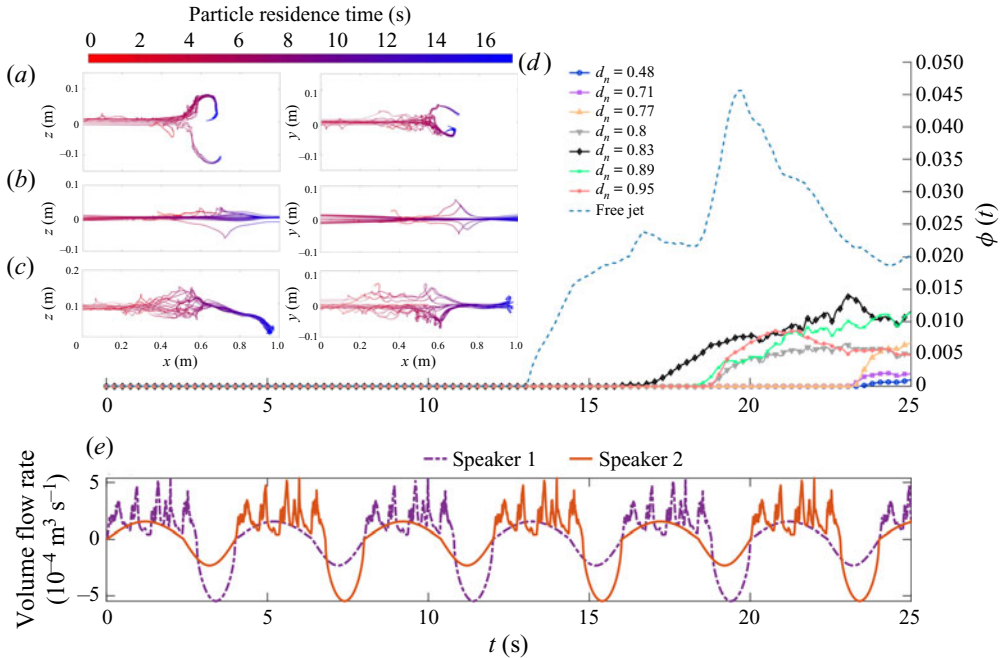


Figure 6. Side and top views of the trajectory of particles with highest streamwise reach for  $L = 1$  m: (a)  $d_n = 0$ , (b) free jet, and (c)  $d_n = 0.83$  (movie 6). (d) Graph showing  $\phi(t) \equiv N_H/N_i$  for different offsets. (e) Volume flow-rate signals for speaker 1 (violet) and 2 (orange).

(figure 3) will be most effective for small  $d_n$ , preventing, for at least short time scales, the particles from reaching the region inhaled in one breath by speaker 2, or zone of influence, which is defined as a hemispherical region of radius 5 cm near the mouth (see § 3 for details). Of course, if  $d_n$  is too large, the particle cloud does not enter the zone of influence, hence does not contribute to virus transmission. Thus, we expect to have a critical value of  $d_n$ , denoted  $d_{nc}$ , for which the risk of transmission is the highest. To quantify the transport of particles from speaker 1 to speaker 2 at  $L = 1$  m, we report the trajectories of the 20 furthest-reaching particles, after four breathing–speaking cycles (17 s) for three values of  $d_n = 0, 0.83$  and  $\infty$  ( $d_n = \infty$  is equivalent to a single free jet, as there is no interaction). For  $d_n = 0$  (figure 6a) the collision is evident, while for  $d_n = \infty$  (figure 6b) the particles travel unobstructed; for both cases the particles are not inhaled.

At an intermediate offset, for instance  $d_n = 0.83$ , the trajectory of the particles is shown in figure 6(c) ( $L = 1$  m). The particles travel downstream with limited lateral deflection until the two jets collide. Upon collision, the particles tend to meander around  $x \approx 0.5$  m until the arrival of the subsequent puffs near 12 s (see movie 6). Thereafter, the meandering is replaced by a coordinated motion of the particles towards speaker 2’s mouth. The motion is largely a consequence of the entrainment due to the exhaled jet from speaker 2 and partly due to the inhalation that ends around 16 s (see movie 10 for details). The particles invade the zone of influence of speaker 2 at  $t \approx 17$  s.

Quantitative trends can be analysed from the number of particles  $N_H$  in the zone of influence, non-dimensionalized by  $N_i$ , the number of particles injected in a breath lasting 4 s. Figure 6(d) displays  $\phi \equiv N_H/N_i$  versus time for a range of offsets,  $d_n \in (0.48, 0.95)$ . Since the particles are unable to reach the zone of influence for  $d_n = 0$  and  $\infty$ , such values are not displayed. The ‘free jet’ in figure 6(d) represents a hypothetical case where

speaker 2 is present, with zero offset, but breathes in a way that does not affect the flow from speaker 1. Although there is no inhalation for speaker 2, we still use a hemisphere of radius 5 cm to calculate  $\phi$ . This case is thus used as a reference to highlight the effectiveness of the blocking effect. In figure 6(d),  $\phi(t)$  reveals that less than 0.5% of the injected particles per breath reach the invasion zone for  $d_n \leq 0.77$ . However,  $\phi$  increases to 1%–1.5% for  $0.77 < d_n < 0.89$ , which implies that the invading particles increase by a factor of 2–3 in an offset range of 1 cm. This result is counterintuitive, as the interaction of the jets can not only block but also assist the invasion of particles into the zone of influence (see movie 10 for details).

### 3. Risk assessment of pathogen inhalation

Conversations are an integral part of our daily lives, and the risk of contracting an airborne disease at a short range is therefore of significant interest. In particular, the probability of infection during an unmasked conversation is yet to be assessed. We have simulated the transient flow field during the initial moments of a conversation. During the period of the simulation, it would be instructive to estimate the probability for a ‘super-titerer’ (a super-titerer is an individual who has an exceptionally high viral load in their saliva) to get an upper bound on the risk of infection for SARS-CoV-2 transmission. However, the same analysis could be performed for any airborne diseases by adapting the virus emission rates.

The probability of infection,  $P$ , is estimated using the equation (Watanabe *et al.* 2010)

$$P = 1 - \exp(-N/N_\infty), \quad (3.1)$$

where  $N$  is the number of virions inhaled and  $N_\infty$  is the characteristic infection dose, which is assumed to be  $5 \times 10^5$  (Poydenot *et al.* 2021). (While many modelling works assume an infection dose of the order of 100 virions (Yang *et al.* 2020; Bazant & Bush 2021), Poydenot *et al.* (2021) stressed that the typical infectious dose is better estimated as  $N_\infty = 5 \times 10^5$ . The present risk assessment follows that of Yang *et al.* (2020), albeit with a corrected infection dose.)

The number of virions inhaled may be quantified based on the average virion concentration field  $\kappa(t)$  in the zone of influence and the average inhalation volume flux  $Q_r$ . We estimate the average droplet volume fraction field,  $\kappa(t)$  (volume of droplets/volume of air), as

$$\kappa(t) = \frac{c_h}{c_i} \kappa_0, \quad (3.2)$$

where  $\kappa_0$  is the volume fraction of droplets at the mouth of speaker 1,  $c_i$  is the injected concentration of particles, and  $c_h = N_H/V_H$  is the concentration of the particles in the hemispherical zone of influence, whose volume is  $V_H = \frac{2}{3}\pi r_h^3$  ( $r_h = 5$  cm for our volume flow rate). The quantity  $\eta \equiv c_h/c_i$  is a measure of the dilution of the particles between what is exhaled by speaker 1 and what is inhaled by speaker 2. Tests on patients infected in early 2020 have shown that the virus concentration in the saliva is  $C_v \approx 7 \times 10^6 \text{ ml}^{-1}$  on average, but may reach  $C_v = 2 \times 10^9 \text{ ml}^{-1}$  (Wölfel *et al.* 2020). Here, we use this latter value as representative of a ‘super-titerer’. Whether such a person becomes a super-spreader or not depends on their social life. The volume fraction of droplets,  $\kappa_0$ , lies in the range  $2 \times 10^{-9}$  to  $1 \times 10^{-8}$  depending upon the loudness of the speech (Yang *et al.* 2020), and we have taken  $\kappa_0 = 1 \times 10^{-8}$ . Hence the number of virions inhaled,  $N(t)$ ,

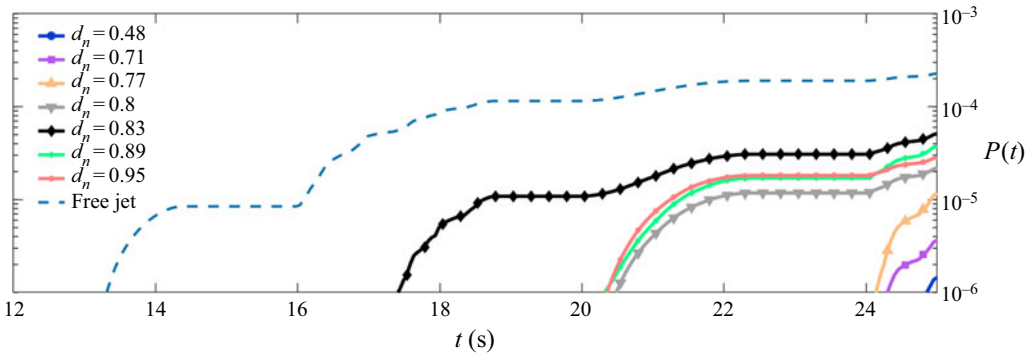


Figure 7. The variation of infection probability  $P(t)$  with speaking time  $t$  for  $L = 1$  m.

can be expressed as

$$N(t) = \int_0^t C_v \kappa(t') Q_r dt'. \quad (3.3)$$

The probability of infection,  $P(t)$ , is shown in [figure 7](#) for different offsets, and the fraction of particles,  $\phi(t)$ , reaching the zone of influence can vary considerably with  $d_n$ . For a super-titerer in the short duration we have simulated, we find that the probability of infection remains below 0.05 % for all offsets. This is certainly a low value, but it is relevant to a conversation of less than 25s. In a longer conversation, the risk is expected to increase, although the flow field and the concentration of virus inhaled will depend upon the phrases spoken and the ambient conditions.

Despite the limitations of our minimal model of a short conversation, we have identified new insights in this study. For instance, one might ask how efficient is the blocking effect? Qualitatively, the flow field and the particle trajectories reveal that the effect is significant, and the quantitative estimate  $\phi$  indicates that the fraction of particles inhaled might be decreased two- to threefold. To quantify the consequences in terms of transmission risks, we compare the probability of infection for various offsets to the hypothetical ‘free-jet’ case. Two consequences of the blocking effect are evident: (i) the infection probability diminishes substantially and (ii) the invasion time is delayed for all the offsets. However, as time progresses, the difference between the ‘free-jet’ and large offsets is reduced. Indeed, it would be interesting to investigate whether the protection due to the blocking effect remains relevant at long times or not.

#### 4. Conclusions

The interaction of respiratory jets emanating from speech and breathing signals has been examined for the initial phase of a two-person conversation, with both experiments and numerical simulations. The role of conversations during social interactions in the transmission of airborne diseases at short range is largely unexplored (Yang *et al.* 2020; Singhal *et al.* 2021), and our study provides insight into the jet collision dynamics and estimation of the virus transport. We characterize the collision of jets using flow visualization images and measurements of the axial and lateral spreading rate of the jet at different offset heights, qualitatively in the experiments and quantitatively using the simulations. The axial spreading is controlled by the time needed for the jets to collide, which largely depends on the horizontal separation of the two speakers. At longer times,

the axial spreading depends on the vertical offset. The time between successive exhalations determines the details of jet arrival at a nearby speaker. With the simulated flow field, we use tracer particles to mimic the airborne transport of droplets containing pathogens, which can be inhaled by a nearby susceptible person (figure 6a–c).

Our analysis revealed a blocking effect that is effective at small offsets, due to the collision of opposing jets, which has a substantial influence on limiting airborne transmission at early times. The details depend on the offset height. There exists a critical window of offsets where the flow field associated with the susceptible person's speech and breathing may entrain infected particles towards a region where they can be inhaled. An indirect consequence of the blocking effect is the enhanced lateral spread of the jets, which suggests air exchange with neighbouring persons, and impacts long-range airborne transmission too. Consequently, the aerosols from an infected speaker may enhance indirect airborne transmission if the face-to-face conversation occurs at a table with multiple individuals, as seen in figure 1(a). Figure 1(a) also illustrates that, when both the speakers are standing, the offset height could be large, and the blocking effect ceases, as the jets do not interact. The strength of breathing and speaking signals may in reality differ, and its consequences on the collision dynamics are as yet unknown.

A long-term goal is to assess the transmission risk associated with the direct transport of virus during a conversation. Our simulations account for realistic details regarding the variation in volume flow rate in speech and breathing, including height offsets. However, a real conversation features additional complexities that need to be understood to propose a risk assessment of direct airborne transmission. Our simulations have clarified the situation where the exhaled flows are directed forwards and are not sensitive to thermal effects. Such flows are relevant to mouth breathing and many spoken syllables. However, buoyancy effects, thermal currents near the human body, inhalation and exhalation flow due to nose breathing (Zhou & Zou 2021) and certain syllables, e.g. those affected by the position of the tongue, will generate flows in other directions and are subjects of future research. In addition, our work has focused on the initial phase of conversations, but longer and varied conversations should be simulated, which may reveal additional phenomena. Finally, estimates of the probability of infection are based on empirical constants, like the characteristic dose  $N_\infty$ , which are themselves an active topic of research (Basu 2020; Smith *et al.* 2020; Poydenot *et al.* 2021). The pandemic has highlighted the crucial role of short-range airborne transmission, which, in turn, has underscored how little we know about the fluid dynamics of the airflows in speech.

**Supplementary material and movies.** Supplementary material and movies are available at <https://doi.org/10.1017/jfm.2021.915>.

**Acknowledgements.** The authors thank R. Adak for helpful discussions and P. Bourriane for help with calibration of the flow rate from the pressure pump.

**Funding.** A.G., N.B. and S.S. acknowledge the National Supercomputing Mission (NSM) for providing computing resources of 'PARAM Shakti' at IIT Kharagpur, which is implemented by C-DAC and supported by the Ministry of Electronics and Information Technology (MeitY) and the Department of Science and Technology (DST), Government of India. H.A.S. thanks the NSF for support via the RAPID Grants Nos CBET 2029370 and CBET 2116184 (Program Manager R. Joslin). D.L.C. acknowledges support from the National Science Foundation Graduate Research Fellowship Program.

**Declaration of interests.** The authors report no conflict of interest.

**Author ORCIDs.**

▣ Arghyanir Giri <https://orcid.org/0000-0002-6069-1371>;

▣ Nan Xue <https://orcid.org/0000-0002-4729-0741>;

- Simon Mendez <https://orcid.org/0000-0002-0863-2024>;  
Sandeep Saha <https://orcid.org/0000-0002-0507-9980>;  
Howard A. Stone <https://orcid.org/0000-0002-9670-0639>.

REFERENCES

- ABKARIAN, M., MENDEZ, S., XUE, N., YANG, F. & STONE, H.A. 2020 Speech can produce jet-like transport relevant to asymptomatic spreading of virus. *Proc. Natl Acad. Sci.* **117** (41), 25237–25245.
- ALLEN, J.G. & IBRAHIM, A.M. 2021 Indoor air changes and potential implications for SARS-CoV-2 transmission. *J. Am. Med. Assoc.* **325** (20), 2112–2113.
- ANDERSON, E.L., TURNHAM, P., GRIFFIN, J.R. & CLARKE, C.C. 2020 Consideration of the aerosol transmission for COVID-19 and public health. *Risk Anal.* **40** (5), 902–907.
- ASADI, S., BOUVIER, N., WEXLER, A.S. & RISTENPART, W.D. 2020 The coronavirus pandemic and aerosols: does COVID-19 transmit via expiratory particles? *Aerosol Sci. Technol.* **54** (6), 635–638.
- BASU, S. 2020 Computational characterization of inhaled droplet transport in the upper airway leading to SARS-CoV-2 infection. medRxiv.
- BAZANT, M.Z. & BUSH, J.W.M. 2021 A guideline to limit indoor airborne transmission of COVID-19. *Proc. Natl Acad. Sci.* **118**, 2–10.
- BESBES, S., MHIRI, H., LE PALEC, G. & BOURNOT, P. 2003 Numerical and experimental study of two turbulent opposed plane jets. *Heat Mass Transfer* **39** (8), 675–686.
- BHAGAT, R.K. & LINDEN, P.F. 2020 Displacement ventilation: a viable ventilation strategy for makeshift hospitals and public buildings to contain COVID-19 and other airborne diseases. *R. Soc. Open Sci.* **7** (9), 200680.
- BHAGAT, R.K., WYKES, M.D., DALZIEL, S.B. & LINDEN, P.F. 2020 Effects of ventilation on the indoor spread of COVID-19. *J. Fluid Mech.* **903**, 14–15.
- BOUROUBA, L. 2020 Turbulent gas clouds and respiratory pathogen emissions: potential implications for reducing transmission of COVID-19. *J. Am. Med. Assoc.* **323** (18), 1837–1838.
- BOUROUBA, L. 2021 The fluid dynamics of disease transmission. *Annu. Rev. Fluid Mech.* **53**, 473–508.
- CHONG, K.L., NG, C.S., HORI, N., YANG, R., VERZICCO, R. & LOHSE, D. 2021 Extended lifetime of respiratory droplets in a turbulent vapor puff and its implications on airborne disease transmission. *Phys. Rev. Lett.* **126** (3), 034502.
- DENSHCHIKOV, V., KONDRAT'EV, V. & ROMASHOV, A. 1978 Interaction between two opposed jets. *Fluid Dyn.* **13** (6), 924–926.
- DUGUID, J.P. 1946 The size and the duration of air-carriage of respiratory droplets and droplet-nuclei. *Epidemiol. Infect.* **44** (6), 471–479.
- FENNELLY, K.P. 2020 Particle sizes of infectious aerosols: implications for infection control. *Lancet Respir. Med.* **8** (9), 914–924.
- GARCIA, W., MENDEZ, S., FRAY, B. & NICOLAS, A. 2021 Model-based assessment of the risks of viral transmission in non-confined crowds. *Saf. Sci.* **144**, 105453. ISSN 0925–7535.
- GREENHALGH, T., JIMENEZ, J.L., PRATHER, K.A., TUFEKCI, Z., FISMAN, D. & SCHOOLEY, R. 2021 Ten scientific reasons in support of airborne transmission of SARS-CoV-2. *Lancet* **397** (10285), 1603–1605.
- GUPTA, J.K., LIN, C.-H. & CHEN, Q. 2010 Characterizing exhaled airflow from breathing and talking. *Indoor Air* **20** (1), 31–39.
- KAYE, N. & LINDEN, P. 2006 Colliding turbulent plumes. *J. Fluid Mech.* **550**, 85–109.
- KLOMPAS, M., BAKER, M.A. & RHEE, C. 2020 Airborne transmission of SARS-CoV-2: theoretical considerations and available evidence. *J. Am. Med. Assoc.* **324** (5), 441–442.
- LI, W., SUN, Z., LIU, H., WANG, F. & YU, Z. 2008 Experimental and numerical study on stagnation point offset of turbulent opposed jets. *Chem. Engng J.* **138** (1–3), 283–294.
- LIU, C., HIGUCHI, H., ARENS, E. & ZHANG, H. 2009 *Control of the microclimate around the head with opposing jet local ventilation*. UC Berkeley: Center for the Built Environment.
- MATHAI, V., DAS, A., BAILEY, J.A. & BREUER, K. 2021 Airflows inside passenger cars and implications for airborne disease transmission. *Sci. Adv.* **7** (1), eabe0166.
- MORAWSKA, L., *et al.* 2020 How can airborne transmission of COVID-19 indoors be minimised? *Environ. Intl* **142**, 105832.
- MORAWSKA, L. & CAO, J. 2020 Airborne transmission of SARS-CoV-2: the world should face the reality. *Environ. Intl* **139**, 105730.
- NG, C.S., CHONG, K.L., YANG, R., LI, M., VERZICCO, R. & LOHSE, D. 2021 Growth of respiratory droplets in cold and humid air. *Phys. Rev. Fluids* **6**, 054303.

## A. Giri and others

- PÖHLKER, M.L., *et al.* 2021 Respiratory aerosols and droplets in the transmission of infectious diseases. [arXiv:2103.01188](https://arxiv.org/abs/2103.01188).
- POYDENOT, F., ABDOURAHAMANE, I., CAPLAIN, E., DER, S., HAIECH, J., JALLON, A., KHOUTAMI, I., LOUCIF, A., MARINOV, E. & ANDREOTTI, B. 2021 Risk assessment for long and short range airborne transmission of SARS-CoV-2, indoors and outdoors, using carbon dioxide measurements. [arXiv:2106.09489](https://arxiv.org/abs/2106.09489).
- PRATHER, K.A., MARR, L.C., SCHOOLEY, R.T., MCDIARMID, M.A., WILSON, M.E. & MILTON, D.K. 2020 Airborne transmission of SARS-CoV-2. *Science* **370** (6514), 303–304.
- PRATHER, K.A., WANG, C.C. & SCHOOLEY, R.T. 2020 Reducing transmission of SARS-CoV-2. *Science* **368** (6498), 1422–1424.
- ROLON, J., VEYNANTE, D., MARTIN, J. & DURST, F. 1991 Counter jet stagnation flows. *Exp. Fluids* **11** (5), 313–324.
- SINGHAL, R., RAVICHANDRAN, S., GOVINDARAJAN, R. & DIWAN, S.S. 2021 Virus transmission by aerosol transport during short conversations. [arXiv:2103.16415](https://arxiv.org/abs/2103.16415).
- SMITH, S.H., SOMSEN, G.A., VAN RIJN, C., KOOIJ, S., VAN DER HOEK, L., BEM, R.A. & BONN, D. 2020 Probability of aerosol transmission of SARS-CoV-2. medRxiv.
- TANG, J.W., MARR, L.C., LI, Y. & DANCER, S.J. 2021 Covid-19 has redefined airborne transmission. *Br. Med. J.* **373**, 1–2.
- TANG, J.W., NICOLLE, A.D., PANTELIC, J., JIANG, M., SEKHR, C., CHEONG, D.K. & THAM, K.W. 2011 Qualitative real-time schlieren and shadowgraph imaging of human exhaled airflows: an aid to aerosol infection control. *PLoS One* **6** (6), e21392.
- WÖLFEL, R., *et al.* 2020 Virological assessment of hospitalized patients with COVID-2019. *Nature* **581** (7809), 465–469.
- WATANABE, T., BARTRAND, T.A., WEIR, M.H., OMURA, T. & HAAS, C.N. 2010 Development of a dose-response model for SARS coronavirus. *Risk Anal.* **30** (7), 1129–1138.
- YANG, F., PAHLAVAN, A.A., MENDEZ, S., ABKARIAN, M. & STONE, H.A. 2020 Towards improved social distancing guidelines: space and time dependence of virus transmission from speech-driven aerosol transport between two individuals. *Phys. Rev. Fluids* **5** (12), 122501.
- ZHOU, M. & ZOU, J. 2021 A dynamical overview of droplets in the transmission of respiratory infectious diseases. *Phys. Fluids* **33** (3), 031301.